Extreme Mechanics Letters 36 (2020) 100650

Contents lists available at ScienceDirect

Extreme Mechanics Letters

journal homepage: www.elsevier.com/locate/eml

The effect of defects on the cyclic behavior of polymeric 3D kirigami structures

Kian Bashandeh [a], Mohammad Humood [a], Jungkyu Lee [b], Mengdi Han [c], Yulin Cui [d], Yan Shi [d], Yonggang Huang [e], John A. Rogers [c], Andreas A. Polycarpou [a,*]

[a] Department of Mechanical Engineering, College of Engineering, Texas A&M University, College Station, 77843-3123, TX, USA
[b] Bruker Nano Surfaces, Eden Prairie, MN 55344, USA
[c] Departments of Materials Science and Engineering, Biomedical Engineering, Chemistry, Mechanical Engineering, Electrical Engineering and Computer Science, Center for Bio-Integrated Electronics, Simpson Querrey Institute for Nano/Biotechnology, Northwestern University, Evanston, IL, 60208, USA
[d] State Key Laboratory of Mechanics and Control of Mechanical Structures, Nanjing University of Aeronautics and Astronautics, Nanjing, 210016, PR China
[e] Departments of Mechanical Engineering and Civil and Environmental Engineering, Northwestern University, Evanston, IL 60208, USA

ARTICLE INFO

Article history:
Received 30 November 2019
Received in revised form 17 January 2020
Accepted 16 February 2020
Available online 18 February 2020

Keywords:
3D kirigami structures
Defects
Extreme compression
Mechanical cycling

ABSTRACT

Recent advances in the assembly of three-dimensional (3D) structures driven by compressive buckling have provided an opportunity to exploit the capability in a broad range of engineering applications. These include microelectromechanical systems, energy storage, and wearable electronic devices. The occurrence of defects during fabrication and assembly, or during operation could impact the performance of the devices. Herein, we investigate the mechanical cycling of structures with different types of structural defects, including the presence of a pre-existing crack, structures with a thinner leg, and a pre-buckled leg. Studies of compressive cycling response of these microscale 3D polymer-based kirigami architectures revealed stiffening behavior for both defective and non-defective structures. Structural densification, developed internal stress, and deformation of the elastomer substrate were the reasons for stiffening. Cyclic compression was performed to 50% and extreme condition of 100 % of the initial height using in-situ scanning electron microscopy. The structures were found to achieve stable hysteretic cycling with steady-state mechanical response after a number of cycles. The deformation behavior, the structure stability under cyclic loading, and the load bearing capability were found to be dependent on the defect type, but they were not catastrophic.

© 2020 Elsevier Ltd. All rights reserved.

1. Introduction

Three-dimensional (3D) architectures have emerged as a promising replacement of conventional two-dimensional (2D) structures, due to their application in nano/micro electromechanical systems (NEMS/MEMS) [1–3], biomedical devices [4,5], energy storage devices [6,7], stretchable and wearable electronics [8,9], robotics [2,10], and elsewhere [11–13]. With recent advances in fabrication techniques, such as strain-induced folding/bending and compressive buckling, inspired by the ancient art of origami/kirigami, various programmed configurations and scales of 3D structures, from sub-micron to macro-scales can be realized from 2D patterns [3,14]. In this work, the compressive forces created by releasing the prestrained elastomer transform the non-bonded regions of 2D precursors into the desired 3D kirigami shapes [15].

The successful implementation of such 3D structures in practical applications requires a high level of efficiency and reliability. For example, the mechanical reliability of MEMS devices is a critical concern that must be considered from design to fabrication, and ultimately functionality [16,17]. The ideal situation for structures in applications such as 3D MEMS, sensors, or energy harvesting devices, is to sustain the external load and associated repeated deformation for extended periods of time. Factors such as geometry and thickness of the structure, the level and number of cyclic loading, and defect-induced degradation during the fabrication process, could limit this lifetime and lead to unwanted malfunctioning of the devices.

In an earlier study, we investigated the mechanical resilience of different geometries of 3D kirigami structures under single compressive loading, and found a strong geometric dependent mechanical behavior in terms of flexibility and elastic recovery [18]. Energy dissipation and durability of these structures under repeated compressive cyclic loading were also examined [19]. The structures demonstrated elastic behavior with minimal hysteresis by compressing to 50% of their height. At the extreme

* Corresponding author.
E-mail address: apolycarpou@tamu.edu (A.A. Polycarpou).

https://doi.org/10.1016/j.eml.2020.100650
2352-4316/© 2020 Elsevier Ltd. All rights reserved.

Table 1
SEM of structures with/without defects tested at 50 and 100% compression.

Structures without defect		*Structures with defect*		
Table	Rotated table	Pre-existing crack	Thinner leg	Pre buckled leg
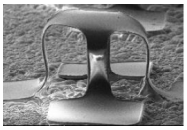		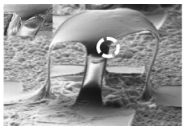	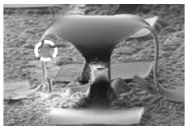	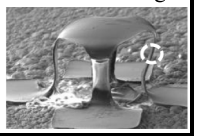

* The dashed circle shows the site of defect in each structure.

condition of cycling to 100% compression, the structures achieved stable hysteresis after few cycles and 94% elastic recovery.

Herein, we investigate the mechanical responses of 3D kirigami-inspired structures with different types of defects. In any microfabrication process, the aim is always to increase the yield. However, sometimes defects are introduced in these structures at different steps of the process. Since buckling is a defect-dependent deformation, it is essential to investigate how these structures behave under compressive loading with the existence of such defects. 3D structures with defects were fabricated using a controlled compressive buckling approach and mechanically tested under cyclic compressive loading using in-situ scanning electron microscopy (SEM).

2. Materials and methods

Fabrication of the 3D structures started with patterning of 2D precursors of epoxy (SU-8, 3 μm thickness) by spin coating and photolithography on a layer of silicon dioxide (SiO_2, 800 nm thickness), which was previously formed on a silicon wafer by thermal oxidation. The exposed regions of the SiO_2 layer were then removed by wet etching in diluted hydrofluoric acid (HF). Spin coating and photolithography were used again to form another layer of photoresist (AZ 5214, 4 μm thickness) on the non-bonded regions of the precursors. The remaining buried SiO_2 layer under the precursors was eliminated by another HF wet etching process, to facilitate the transfer printing of the precursors from the Si wafer to another silicone elastomer substrate (Dragon Skin®, 600 μm thickness). A layer of titanium (5 nm thickness) and SiO_2 (50 nm thickness) were deposited on the precursors by electron beam evaporation to enhance the adhesion of the bonding regions of the precursors with the elastomer substrate.

The 2D patterns were then transfer printed from the Si wafer to a water-soluble polyvinyl alcohol (PVA) tape using a polydimethylsiloxane (PDMS) stamp. To form a strong bonding between the elastomer substrate and the precursors, the silicone elastomer and the precursors on the PVA tape were exposed to ultraviolet-induced ozone treatment, which formed a hydroxyl termination. The elastomer was then biaxially stretched to 75% prestrain with a mechanical stage. The PVA tape and the 2D precursors were then laminated on the stretched elastomer substrate and baked at 70 °C for 8 min to yield a strong bond between the substrate and the bonding regions of the precursors. Thereafter, the PVA tape and photoresist layer were removed using hot water and acetone, respectively. Releasing the pre-strained elastomer substrate induced compressive forces which enabled the out-of-plane deformation of the non-bonded regions of the precursors, forming the desired 3D shapes. A schematic representation of the 2D patterns and their transformation to 3D structures upon releasing the elastomer is illustrated in Fig. 1, for a table structure without defect and with a crack type defect. The crack was formed during the assembly process with a length of ∼10 μm. Each resulting nominal kirigami structure is made of 3 μm thickness SU-8, and a height of 60 μm.

The mechanical cyclic compression experiments were carried out on the structures with/without defects (shown in Table 1) using a commercial PI 88 SEM Picoindenter (Bruker) equipped with a diamond flat punch probe with a diameter of 100 μm. The samples were sputter-coated with 8 nm of Pt/Pd for better visualization inside the SEM. Displacement-controlled mode was used to compress the structures to 50% and 100% of their initial height. The experiment at 50% compression was performed to enable direct comparison between structures with and without defect. Since there was no observable change in the structural performance, extreme compression of 100% was chosen for the other structures.

3. Results and discussion

3.1. Stiffening of the structures at 100% compression

Fig. 2(a, b) show the load–displacement curves obtained by cycling of the rotated table structure to 100%. The curves in Fig. 2(b) were divided for each set for clarity. Three sets of cycling experiments were carried out. Each set consisted of 10 cycles resulting in a total number of 30 cycles. 4 min was selected as the wait time after the complete unloading of the structure at the end of each set to allow for viscous relaxation of the structure/substrate. Note that the structure was fully unloaded only at the last cycle of each test set. The first cycle of each set, particularly set 1, demonstrated the largest hysteresis loop with the highest energy dissipation. This could be due to plastic deformation and initiation of buckling of the leg at the first cycle. Less energy was dissipated in subsequent cycles, indicating stabilization of the structure.

The load bearing capacity increased with each set, as shown in Fig. 2(b). The curves showed three regions for the loading associated with Hookean-type deformation with a linear slope, a reduction in the slope due to small buckling, and an increase in the slope due to stiffening of the structure. Similar behavior was observed for single compression of kirigami structures [18]. The reasons behind the stiffening can be attributed to different mechanisms involved during the compression of the structure. Referring to the recorded movie S1 in the supporting information, the densification of the structure with increase in compression forced the legs to ultimately touch the bonding pads and the substrate, wherein rapid increase in the force with small compression was initiated. According to [20], a slight curvature in a thin sheet can significantly increase the stiffness during bending, due to developed internal stresses. Here, the bonding pads behaved similar to a curved thin sheet subjected to bending at 100%. The role of substrate deformation became more dominant upon compression to 100%. The compression of the substrate indicated higher stiffness and load bearing capability, compared to the structure [19].

The recorded movie S1 shows that a combination of sliding, twisting, and slight bucking occurred with compression to 100%. The permanent buckling of the leg, and twisting of the structure can also be observed from the SEM images shown in Fig. 2(c),

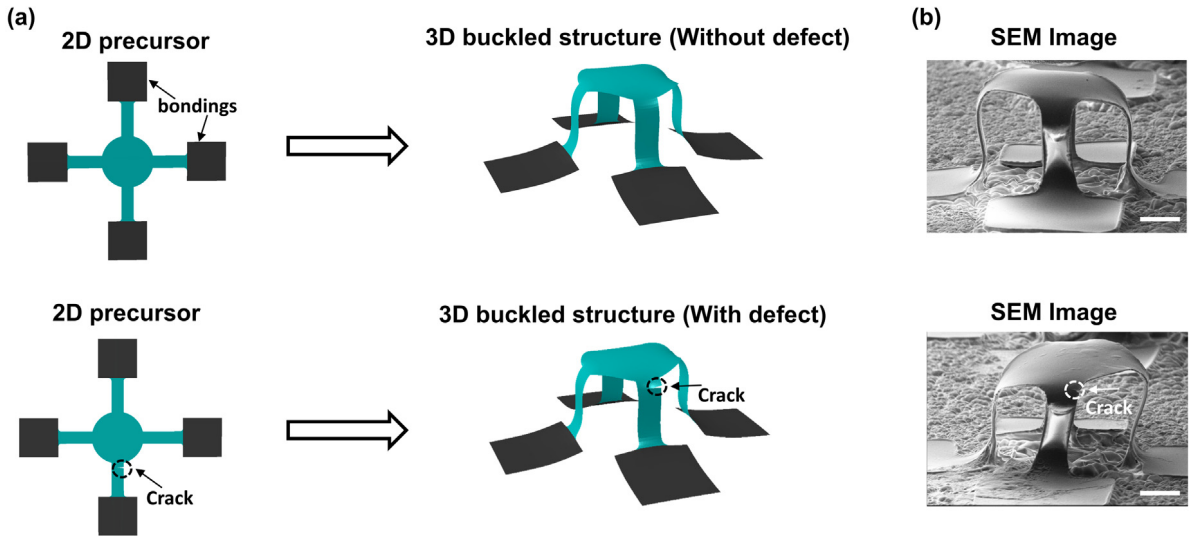

Fig. 1. (a) Schematic illustration of 2D design patterns and 3D kirigami structures assembled by controlled buckling, and (b) SEM images of the fabricated structures (scale bar is 25 μm).

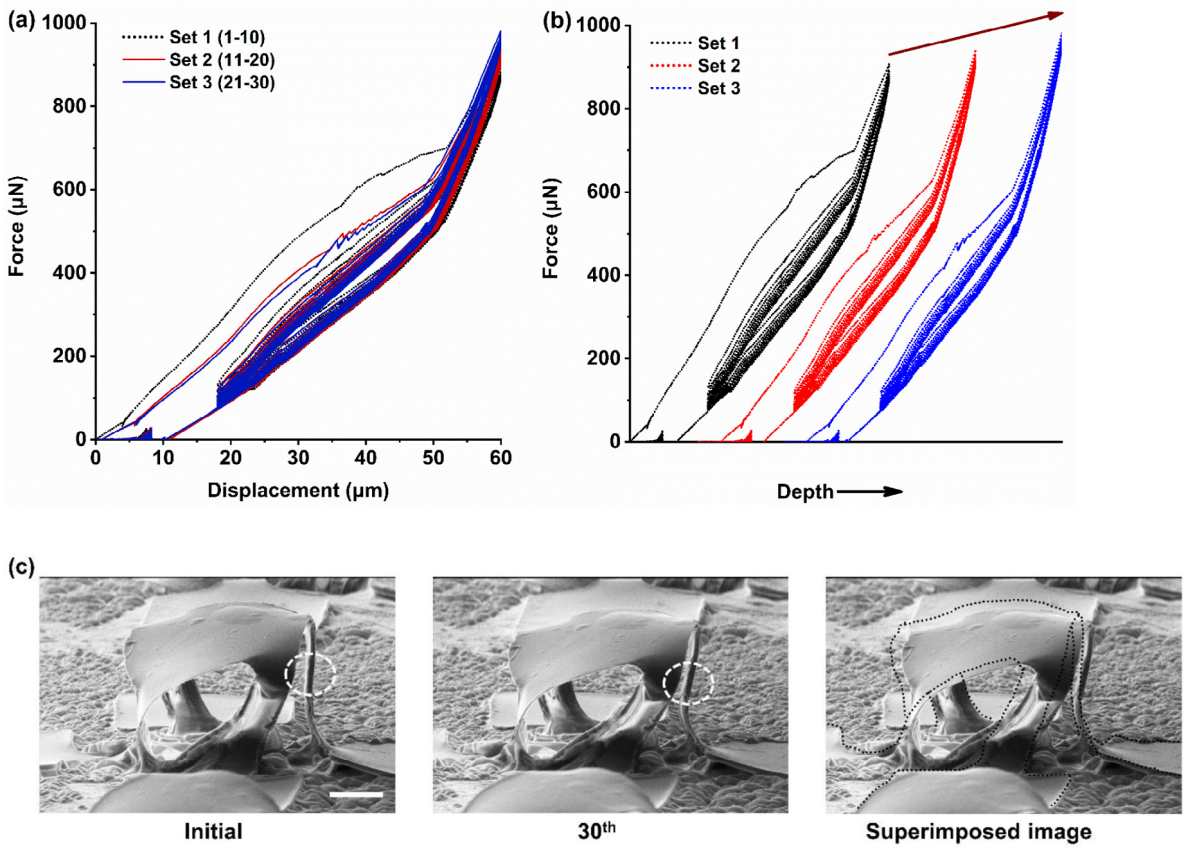

Fig. 2. Rotated table structure without defect: (a) Load–displacement curves for 30 cycles of loading-unloading, compressed to 100%, (b) Separated cycling curves for each set, and (c) SEM images taken before and after 30 cycles, including superimposed initial and deformed structure (scale bar is 25 μm).

which were taken before the experiment started and after the 30th cycle. The buckling of the leg is shown with a dashed white circle in the SEM images. The superimposed image depicts a better visualization of the changes in the shape of the structure after the experiments. The dashed black line represents the initial structure before the experiment. From the superimposed image in Fig. 2(c), three distinct deformation modes can be observed: (a) shifting to the right in the sliding direction, (b) slight reduction in the height due to buckling of the leg, and plastic deformation, and (c) in-plane twisting of the structure.

3.2. Structures with defects

3.2.1. Structure with crack

The successful implementation of such 3D structures to practical applications such as 3D MEMS sensors requires high reliability

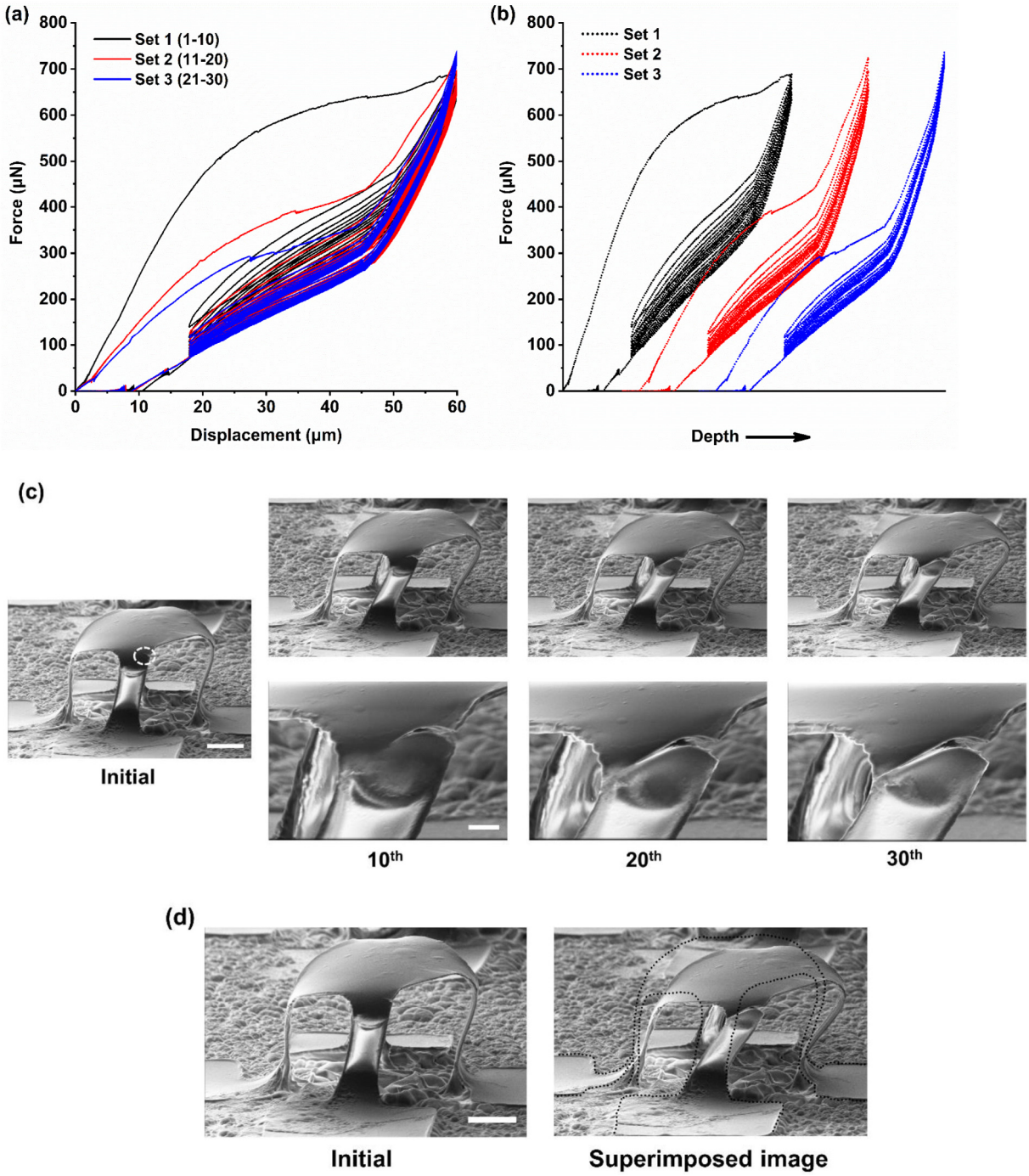

Fig. 3. (a) Table structure load–displacement curves for 30 cycles compressed to 100%, (b) Separated cycling curves for each set, (c) SEM images taken before cycling and after each set of cycles (scale bar is 25 μm for the low magnification images and 5 μm for the high magnification images), and (d) Superimposed SEM images before the experiment and after the 30th cycle (scale bar is 25 μm).

and stability of the structures operating under cyclic mechanical loading. Such loading conditions can induce fatigue in the structure, which can ultimately lead to cracking and failure. In Ref. [19], we investigated the mechanical response of a rotated table structure subjected to 200 cycles under extreme compression of 100%. The formation and growth of a microcrack were observed after the 100th cycle. Herein, the structure had a pre-existing crack in one of the legs to capture a crack-type defect that could occur during the fabrication process. Similar to our prior study, the crack formed at the ribbon-membrane connection, which turns out to be the more sensitive location for crack formation.

Three sets of cyclic experiments with ten cycles at each set were conducted at 100% compression on a table structure with a small crack on its front leg, depicted with a white dashed circle in Fig. 3(c). Fig. 3(a, b) show the load–displacement curves at each set. Initially, the structure demonstrated a Hookean response with linear elastic behavior followed by a large increase in the displacement with little increase in the load due to rapid buckling. Finally a large increase in the load due to stiffening when the structure approached 100% compression. The first cycle showed the highest energy dissipation, while less energy was dissipated in the first cycle of the 2nd and 3rd sets. The structure achieved stable hysteresis and stabilized with increasing number of cycles.

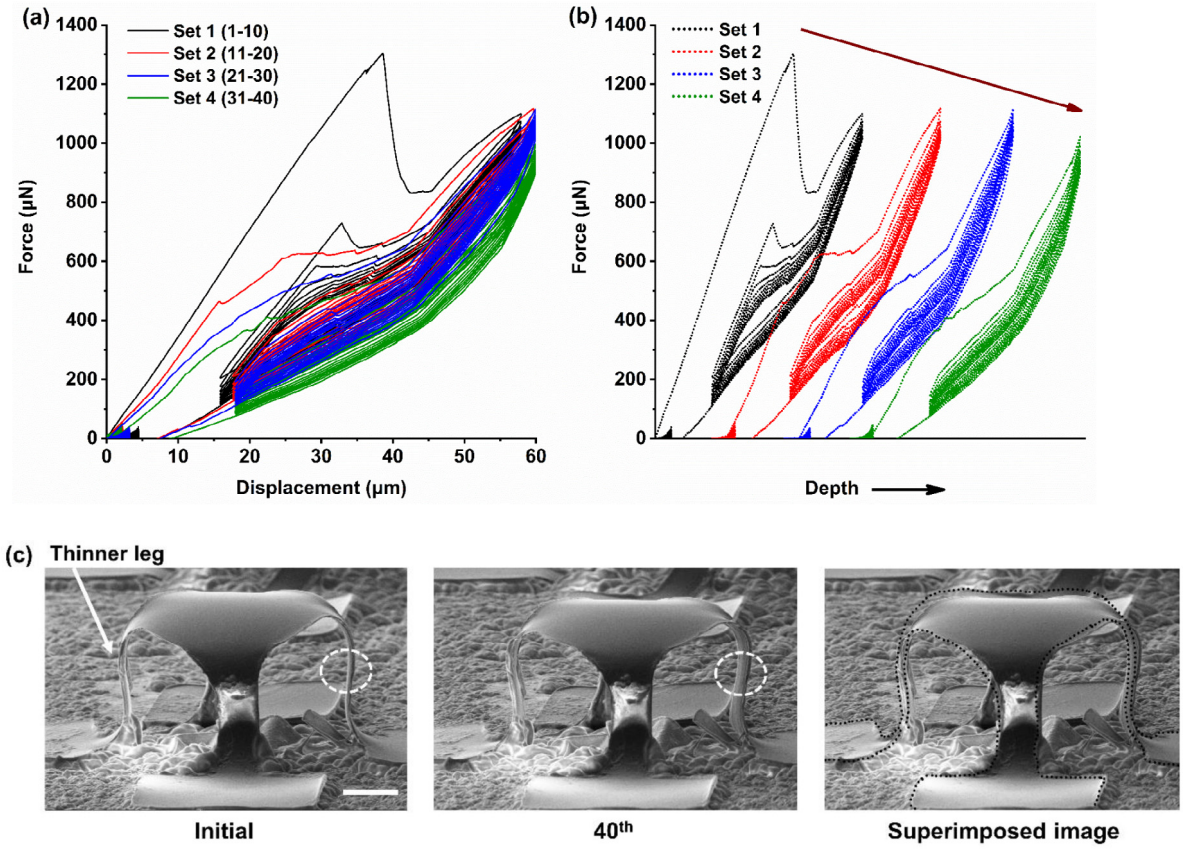

Fig. 4. (a) Table structure load–displacement curves for 40 cycles at 100%, (b) Separated cycling curves for each set, and (c) SEM images taken before and after 40th cycles, including superimposed initial and deformed structure (scale bar is 25 μm).

The structure became more robust and resistant to crack growth at subsequent sets.

A combination of sliding and buckling occurred during the compression to 100% (see the recorded movie S2 for the first set). The buckling of the leg and permanent deformation of the structure is clearly discernible from the movie S2, as well as the SEM images shown in Fig. 3(c, d). Fig. 3(c) shows the SEM images of the structure taken before the experiment and after each set of cycling tests. The higher magnification images show the growth of the crack with cyclic compression at each set. The comparison of the images after sets 2 and 3 (the 20th and 30th cycle) indicate negligible growth in the crack, compared to the 10th cycle. The developed internal tensile stress on the leg resulted in the crack growth. As seen in movie S2, the top portion of the leg is under tension with buckling of the leg inducing tensile stress at the crack site. The internal stresses decreased with number of cycles, which caused the crack growth to decelerate [21]. Fig. 3(d) depicts the superimposed image before the experiment and after the 30th cycle. The structure permanently deformed and tilted in the sliding direction, and the right leg experienced two-fold bending.

3.2.2. Structure with thinner leg

Numerical analysis of structures with different thicknesses showed the dependence of the mechanical response on the thickness of the structure [19]. Structures with lower thickness demonstrated a more compliant behavior with lower load bearing capacity and stiffness. Here, the thickness effect is incorporated as a defect in the structure. The structure was compressed for 40 cycles at 100%. The respective load–displacement curves are depicted in Fig. 4(a, b). During the first cyclic loading, the structure followed a linear elastic behavior up to a threshold, where a sudden drop in the load occurred. Referring to the recorded movie S3, this sudden drop was accompanied by an instantaneous in-plane twisting and sliding of the structure as well as buckling of the right leg. The permanent twisting/buckling can also be observed in the SEM images depicted in Fig. 4(c). The right leg marked with a dashed white circle and the superimposed image before and after the experiments show the twisting/buckling in the legs. The sudden slip/twisting/buckling occurred due to the asymmetric supporting of the load by the legs. Subsequent cycling demonstrated a stable hysteresis with minimal degradation of the structure due to post-buckling/twisting stability. The load bearing capability decreased after each set, particularly between 1st and 2nd sets.

3.2.3. Structure with pre-buckled leg

Fig. 5(a) shows the cycling of a table structure without defect, which was carried out in an earlier study for 30 cycles at 50% compression [19]. The structure demonstrated a linear elastic behavior with minimal energy dissipation and stable hysteresis with complete recovery between each set. The defect considered in this section was introduced to the structure as buckling on one of the legs during the compressive buckling process. Fig. 5(b) shows the cycling behavior of the structure at 50% for five sets; each set consisted of 10 cycles. The maximum force dropped in the first cycle and then stabilized in subsequent cycles within each set. The load bearing capability decreased between each set, as revealed by the downward shifting of the curves. In contrast to the structure without defect, the structure with defect dissipated higher energy and did not stabilize by the end of cycling tests. The load bearing capacity decreased by 37%, compared to the structure without defect. According to the recorded movie S4, the deformation was accompanied by sliding due to the asymmetric

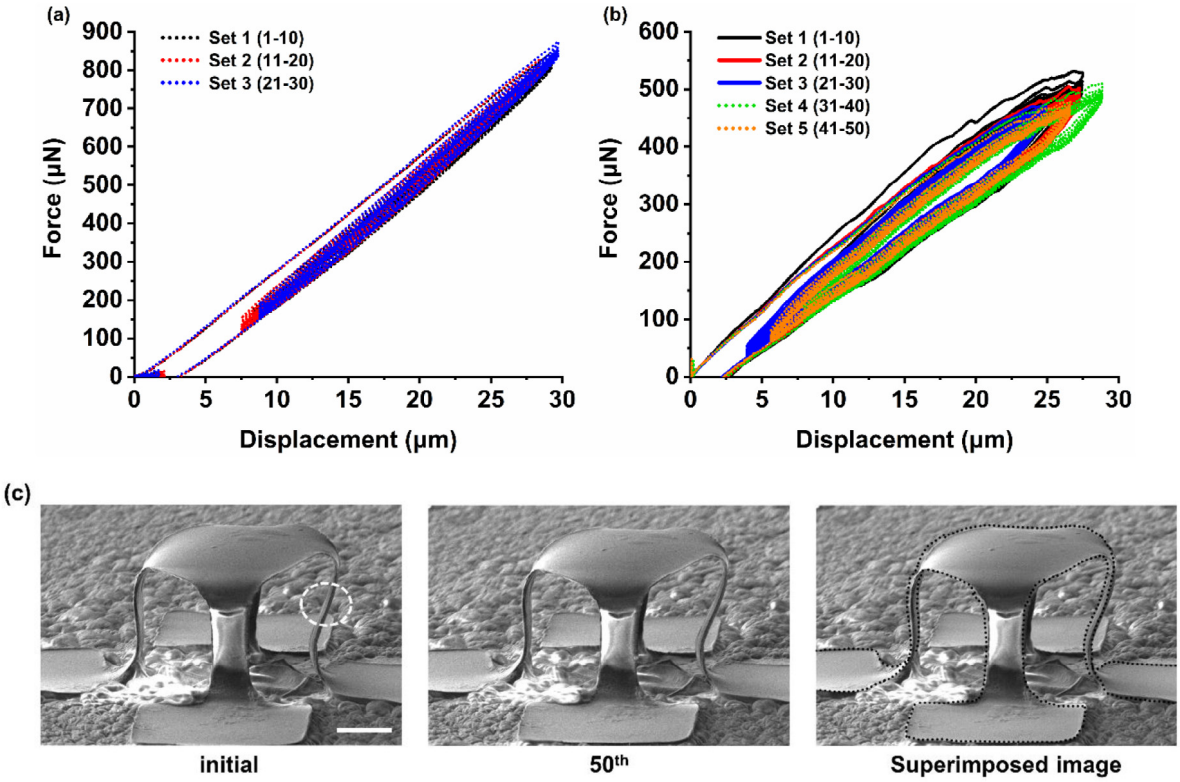

Fig. 5. Table structure load–displacement curves for cycling at 50% compression (a) no defect [19], (b) pre-buckled leg defect, and (c) SEM images taken before cycling and after 50 cycles, including superimposed initial and deformed structure (scale bar is 25 μm).

support of the load by the legs. The buckled leg is marked in Fig. 5(c) with a white dashed circle. The structure experienced a slight change in its shape in the sliding direction, as can be seen from the superimposed image.

3.3. Modeling using finite element analysis (FEA)

3D FEA was conducted using the commercial software ABAQUS to simulate the structures with different types of defects. The goal was to investigate and compare the variations in configuration and stress/strain distributions upon compression to 100%. The structures and the elastomer substrate were simulated using four-node shell elements and eight-node 3D stress elements, respectively. The convergence of mesh size ensured computational accuracy. The SU8 kirigami structures were assumed to be linear elastic with elastic modulus E and Poisson's ratio ν of $E_{SU8} = 4.02$ GPa and $\nu_{SU8} = 0.22$, respectively. Mooney Rivlin hyper-elastic model was used to model the elastomeric substrate with parameters $C_{10} = 0.06757$ MPa, $C_{01} = 0.01689$ MPa, and $D_1 = 0.48$ MPa^{-1}. The length for the legs of the structures were measured to be 55 μm, except the structure with pre-buckled leg defect, which was 65 μm. All legs had a thickness of 3 μm, except the structure with thinner leg defect, which had a thickness of 2.1 μm on its thinner leg.

Fig. 6 shows the maximum principal strain and von Mises stress at 100% compression for the structure without defect and the structures with different types of defects. For all structures except the structure with the pre-existing crack, the maximum strain and von Mises stress developed at the ribbon-membrane connections. The crack tip experienced the highest stress among the structures. The structure with thinner leg defect experienced the highest strain at the thinner leg with bending dominated deformation. The structure with pre-buckled leg showed similar strain behavior to non-defective structure, but higher stress at the top membrane-ribbon connection. All the structures exceeded the fracture threshold of SU8 (≈10%), leading to permanent plastic deformation in the legs.

4. Conclusion

Extreme mechanical cycling of 3D kirigami-inspired architectures with defects was performed using in-situ SEM flat punch compression at 50 and 100%. Three different types of structural defects, which could result during batch fabrication, were considered during the compressive buckling process. Apart from the possibility of occurrence of defects in the assembly process, these defects might also occur in practical applications during operation under extreme conditions. Therefore, it would be beneficial to know how the existence of defects would impact the mechanical response and durability against compressive cycling. Reduction in load bearing capacity, energy dissipation, and deformation of the structures were found to be a function of the defect type. The crack type defect created a large plastic deformation in the sliding direction. The thinner leg type defect caused a sudden snap during the first cycle with a slight permanent twisting remaining after the experiments. The structures maintained stable hysteresis and achieved post-buckling stability after a few cycles, which is advantageous. Compared to the structure without defect, the pre-buckled leg in the structure induced non-instability in the load–displacement response with higher energy dissipation and decreased load bearing capacity by 37%. The degree of plastic deformation was found to be a function of defect type. The existence of crack in one of the legs caused the largest plastic deformation. A common characteristic between the investigated 3D structures and other 3D kirigami structures is their beneficial compliance and elasticity, although variations exist based on the specific structure design (since the stresses generated are geometry dependent). FEA results showed the dependency of stress/strain

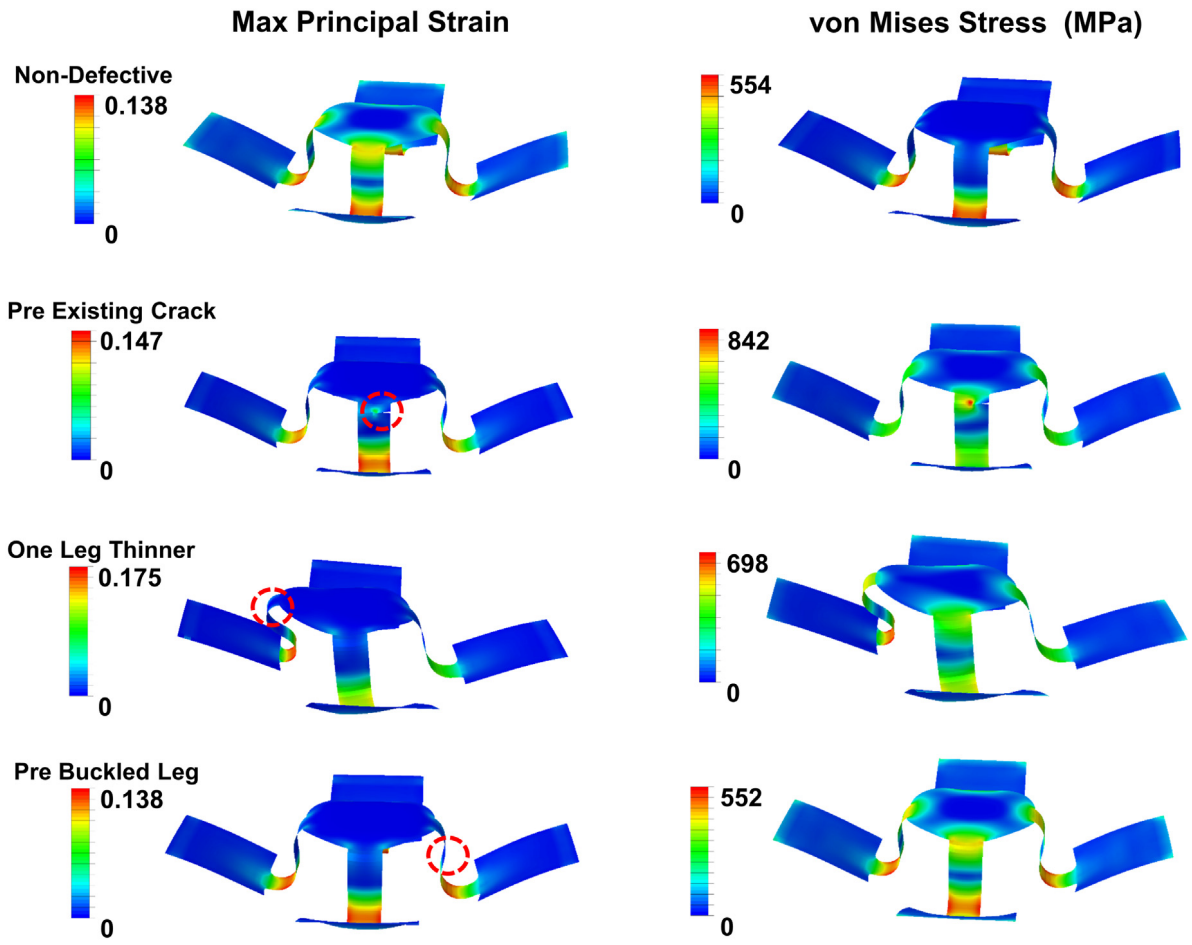

Fig. 6. FEA results for single compression to 100% for the structures with and without defects. The dashed circle shows the site of defect in the structure.

distribution and deformation on the defect type. The internally developed stress and the deformation of the substrate were the mechanisms behind stiffening, once compressed to 100%. It is worth noting that despite the defect type, all structures ultimately achieved stable hysteresis with steady-state mechanical behavior, which is advantageous in practical applications, as they do not lead to catastrophic failures.

Declaration of competing interest

The authors declare that they have no known competing financial interests or personal relationships that could have appeared to influence the work reported in this paper.

Acknowledgments

Funding of this study was provided from the Hagler Institute for Advanced Study (HIAS) at Texas A&M University, USA. Kian Bashandeh acknowledges the support of HIAS through the HEEP graduate fellowship program at Texas A&M University, USA.

Appendix A. Supplementary data

Supplementary material related to this article can be found online at https://doi.org/10.1016/j.eml.2020.100650.

References

[1] C. Wang, L. Taherabadi, G. Jia, M. Madou, Y. Yeh, B. Dunn, C-MEMS for the manufacture of 3D microbatteries, Electrochem. Solid-State Lett. 7 (2004) A435, http://dx.doi.org/10.1149/1.1798151.

[2] S. Felton, M. Tolley, E. Demaine, D. Rus, R. Wood, A method for building self-folding machines downloaded from, Science 345 (2014) 644–646, http://dx.doi.org/10.1126/science.1252610.

[3] J.A. Rogers, Y. Huang, O.G. Schmidt, D.H. Gracias, Origami MEMS and NEMS, MRS Bull. 41 (2016) 123–129, http://dx.doi.org/10.1557/mrs.2016.2.

[4] C.L. Randall, E. Gultepe, D.H. Gracias, Self-folding devices and materials for biomedical applications, Trends Biotechnol. 30 (2012) 138–146, http://dx.doi.org/10.1016/J.TIBTECH.2011.06.013.

[5] B. Tian, J. Liu, T. Dvir, L. Jin, J.H. Tsui, Q. Qing, et al., Macroporous nanowire nanoelectronic scaffolds for synthetic tissues, Nat. Mater. 11 (2012) 986–994, http://dx.doi.org/10.1038/nmat3404.

[6] Z. Song, T. Ma, R. Tang, Q. Cheng, X. Wang, D. Krishnaraju, et al., Origami lithium-ion batteries, Nature Commun. 5 (2014) 3140, http://dx.doi.org/10.1038/ncomms4140.

[7] M.R. Lukatskaya, B. Dunn, Y. Gogotsi, Multidimensional materials and device architectures for future hybrid energy storage, Nature Commun. 7 (2016) 12647, http://dx.doi.org/10.1038/ncomms12647.

[8] J.A. Rogers, T. Someya, Y. Huang, Materials and mechanics for stretchable electronics, Science 327 (2010) 1603–1607, http://dx.doi.org/10.1126/science.1182383.

[9] Y. Su, X. Ping, K.J. Yu, J.W. Lee, J.A. Fan, B. Wang, et al., In-plane deformation mechanics for highly stretchable electronics, Adv. Mater. 29 (2017) 1604989, http://dx.doi.org/10.1002/adma.201604989.

[10] J.C. Breger, C. Yoon, R. Xiao, H.R. Kwag, M.O. Wang, J.P. Fisher, et al., Self-folding thermo-magnetically responsive soft microgrippers, ACS Appl. Mater. Interfaces 7 (2015) 3398–3405, http://dx.doi.org/10.1021/am508621s.

[11] M. Schumann, T. Bückmann, N. Gruhler, M. Wegener, W. Pernice, Hybrid 2D–3D optical devices for integrated optics by direct laser writing, Light Sci. Appl. 3 (2014) e175, http://dx.doi.org/10.1038/lsa.2014.56.

[12] J.L. Silverberg, A.A. Evans, L. Mcleod, R.C. Hayward, T. Hull, C.D. Santangelo, et al., Using origami design principles to fold reprogrammable mechanical metamaterials, Science 345 (2014) 647–650, http://dx.doi.org/10.1126/science.1252876.

[13] Z. Yan, F. Zhang, F. Liu, M. Han, D. Ou, Y. Liu, et al., Mechanical assembly of complex, 3D mesostructures from releasable multilayers of advanced materials, Sci. Adv. (2016) e1601014, http://dx.doi.org/10.1126/sciadv.1601014.

[14] Z. Yan, M. Han, Y. Yang, K. Nan, H. Luan, Y. Luo, et al., Deterministic assembly of 3D mesostructures in advanced materials via compressive buckling: A short review of recent progress, Extrem. Mech. Lett. 11 (2017) 96–104, http://dx.doi.org/10.1016/J.EML.2016.12.006.

[15] S. Xu, Z. Yan, K. Jang, W. Huang, H. Fu, J. Kim, et al., Assembly of micro/nanomaterials into complex, three-dimensional architectures by compressive buckling, Science 347 (2015) 154–159, http://dx.doi.org/10.1126/science.1260960.

[16] J. Iannacci, Reliability of MEMS: A perspective on failure mechanisms, improvement solutions and best practices at development level, Displays 37 (2015) 62–71, http://dx.doi.org/10.1016/J.DISPLA.2014.08.003.

[17] V. Mulloni, B. Margesin, P. Farinelli, R. Marcelli, A. Lucibello, G. De Angelis, Cycling reliability of RF-MEMS switches with Gold–Platinum multilayers as contact material, Microsyst. Technol. 23 (2017) 3843–3850, http://dx.doi.org/10.1007/s00542-015-2782-2.

[18] M. Humood, Y. Shi, M. Han, J. Lefebvre, Z. Yan, M. Pharr, et al., Fabrication and deformation of 3D multilayered kirigami microstructures, Small 14 (2018) 1703852, http://dx.doi.org/10.1002/smll.201703852.

[19] M. Humood, J. Lefebvre, Y. Shi, M. Han, C.D. Fincher, M. Pharr, et al., Fabrication and mechanical cycling of polymer microscale architectures for 3D MEMS sensors, Adv. Eng. Mater. 21 (2019) 1801254, http://dx.doi.org/10.1002/adem.201801254.

[20] V. Pini, J.J. Ruz, P.M. Kosaka, O. Malvar, M. Calleja, J. Tamayo, How two-dimensional bending can extraordinarily stiffen thin sheets, Sci. Rep. 6 (2016) 29627, http://dx.doi.org/10.1038/srep29627.

[21] A. Vasudevan, K. Sadananda, Analysis of fatigue crack growth under compression–compression loading, Int. J Fatigue 23 (2001) 365–374, http://dx.doi.org/10.1016/S0142-1123(01)00172-4.